Applied Physics A (2020) 126:610
https://doi.org/10.1007/s00339-020-03795-w

Applied Physics A
Materials Science & Processing

The effect of various fuels on the yield, structural and optical properties zinc zirconate nanocomposite

M. K. Musembi[1,2] · F. B. Dejene[1] · I. Ahemen[1,3] · K. G. Tshabalala[1]

Received: 7 May 2020 / Accepted: 6 July 2020

Abstract
Various types of fuels were used in a low-temperature solution combustion synthesis of zinc zirconate nanocomposite at a pH of 7. In the synthesis, the fuels used were citric acid, glycine, urea, hydrazine hydrate, and ammonium nitrate while zirconium butoxide and zinc nitrate were the precursor sources of Zr^{4+} and Zn^{2+} ions, respectively. The samples were calcined for 2 h at a temperature of 600 °C. The study of the structural properties showed varied morphologies ranging from highly agglomerated surfaces, crystalline aggregates as well as nanorods. There was a gradual growth of zinc zirconate perovskite within phases of zirconia and zinc oxide. It was observed that there were prominent photoluminescence emissions spread from violet-blue into the yellow-white regions with peaks varying from about 400 to 490 nm. The energy bandgap of the nanocomposites was between 2.93 and 3.22 eV depending on the fuel used in the preparation of the sample.

Keywords Nanocomposite · Stoichiometric fuel ratio · Zinc zirconate · Solution combustion synthesis · Perovskite

1 Introduction

Nanomaterials have unique surface features such as large surface area-volume ratios arising from their reduced crystallite sizes accompanied by extra energy of the surface and densification of the material. These surface characteristics have resulted into unique properties which have generated a lot of interest among scientists [1–3]. Nanocomposite materials exhibit a combination of properties inherent in the individual constituent compounds. Quite often, these properties are more enhanced than those of the individual compounds of the composite and are usually dominated more by the interface or interphase characteristics. It has been observed that there is easy and perfect growth of multiple phases in a nanocomposite when the phases are miscible because of the free diffusion into each other [3–5].

With promising results, scientists have made great efforts in the exploration of various ways of synthesizing nanocomposites, though the traditional mixing and milling methods have still remained the most prominent technologies for the synthesis of single and multiple phase nanocomposite powders at industrial level [3]. Factors that influence the choice and viability of a synthesis route are the type of product needed (e.g. powder, film), the method's simplicity, safety, cost, and rate of production as well as the possibility of large-scale production [6, 7].

Solution combustion synthesis (SCS) is one of the most effective wet chemical methods of synthesizing nanoparticles. The SCS method involves redox reactions between metal oxidants and suitable reducing agents that are used as fuels in the synthesis. In SCS, well dispersed homogenous nanoparticles are produced when precursor solutions are heated to self-combustion. The gases evolved in these reactions assist in the regulation of the final temperature attained through dissipation of the heat energy produced. The exothermic reactions in the synthesis are self-sustaining hence the method is fast, convenient and energy saving.[6, 8–10].

SCS systems may be classified in terms of the solvent used, the oxidizer, and fuel involved. In SCS, water is the commonly used solvent due to its abundance as well as ability to dissolve most organic fuels and nitrates without any secondary reactions taking place. The most common

✉ M. K. Musembi
mchmusembi@yahoo.com

[1] Department of Physics, University of the Free State (QwaQwa campus) Private Bag, X13, Phuthaditjhaba 9866, South Africa

[2] Department of Physical Sciences, Machakos University, Machakos, Kenya

[3] University of Agriculture, Makurdi, Nigeria

Published online: 14 July 2020

oxidizers are metal nitrates, though in some cases, metal hydroxides or chlorides are as well used. A good oxidizer decomposes easily at low temperatures releasing active oxygen [11]. An appropriate fuel is not only an easy source of carbon and hydrogen atoms but one that is characterized by a low decomposition temperature [12]. Such a fuel should mix and easily form complexes with metal ions, thereby facilitating the homogeneity of the cations in the solution. The fuel should readily dissolve in the solvent without leaving any residual mass once decomposed. Nitrogen compounds and salts are not classified as fuels though they have been found to assist in combustion and in aiding the formation of fine nanoparticles by the prevention of agglomeration [6, 13, 14].

There is no best fuel which may be used successfully in all combustion reactions but there is still the best choice in relation to the type of compound being prepared and its specific application. Common substances classified as potential fuels include citric acid, glycine, urea, hydrazine hydrate, carbohydrazide, oxalyl dihydrazide, glycerol, sucrose and some metal acetates. Deganello and Tyagi [14] found out that the amino containing fuels are more redox active, followed by compounds with the –OH group, then the –COOH. Further, it has been found that fuels with reducing valences (RV) greater than 18 usually need some extra thermal treatment at high temperatures in order to remove the residual carbonaceous content [15].

Urea (RV + 6) is a commonly used SCS fuel that has two amino groups attached to a ketone group. When urea is used in SCS as a fuel, it favors the precipitation of metal cations inside the gel during combustion, causing nucleation and extended agglomeration of the particles. Citric acid (RV + 18) is a low-cost nitrogen free and high carbon fuel that consists of one hydroxyl and three carboxylic groups. Citric acid is known for coordinating many metal ions and the evolution of lots of gases that lead to superior powder properties. Being a strong reducing fuel, hydrazine (mono) hydrate (RV + 4) is a fuel that consists of two amino groups capable of explosive combustion mixtures that leave no carbon residue in the final product. Its use is convenient when there is need for high control in the oxidation state. Glycine (RV + 9) is a cheap fuel with a carboxyl and an amino group at its two ends. By effectively forming complexes with metal ions of varying ionic sizes and valences, glycine prevents the selective precipitation and maintains the compositional homogeneity among the constituents [14, 15].

In SCS, the oxidizer/fuel ratio, φ is an important factor that determines the optimum ratio of the oxidants to the fuel in the mixture, where

$$\text{Oxidiser-fuel ratio, } \varphi = \frac{\sum(\text{Coefficients of oxidising elements in formula} \times \text{Valency})}{(-1)\sum(\text{Coefficients of redusing elements in formula} \times \text{Valency})} \quad (1)$$

When $\varphi = 1$, the mixture is stoichiometric while fuel deficient if $\varphi > 1$ and fuel rich when $\varphi < 1$. Studies have shown that maximum combustion energy is released at the stoichiometric oxidizer/fuel ratios [6, 11, 16]. Alves et al. [6] noted that despite the many SCS studies emphasizing the characterization of the synthesized materials, there is very little information on the parameters of combustion such as the fuel effect. This study investigates the effect of using stoichiometric amounts citric acid, glycine, urea, hydrazine hydrate and ammonium nitrate on the nanocomposite properties. The synthesized powders were examined in order to establish the composition, yield, structural, and optical properties of the various phases of the nanocomposite. To the best of our knowledge, the effect of various types of fuel has not been investigated in the synthesis of zinc zirconate nanocomposite.

2 Materials and methods

Figure 1 illustrates the synthesis process of the nanocomposite, which was discussed in greater detail in our earlier work [17]. Analytical grade zinc nitrate (> 99% purity) from Merck and zirconium butoxide (> 99%) from Aldrich were used in this synthesis. The combustion synthesis was initiated by oxidizing zirconium (IV) butoxide with concentrated nitric acid in a fume chamber into completion. The resulting solution was mixed with zinc nitrate that had been dissolved in de-ionised water. To optimize the redox reactions, the appropriate amount of the various fuels was added into either of the nine solutions to achieve the stoichiometric oxidizer-fuel ratio, then the pH adjusted to 7 using ammonia

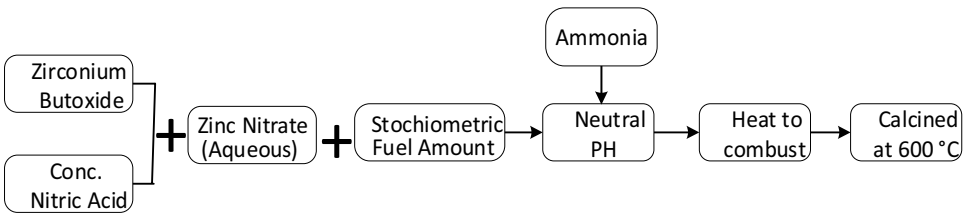

Fig. 1 Schematic stoichiometric synthesis of the composite using different fuels

solution. In order to maintain homogeneity at molecular level, the mixtures were stirred continuously as they were being heated until self-combustion. Each of the resulting fluffy powders was crushed then calcined at 600 °C for two hours in air.

A Phillips Bruker D8 X-ray diffractometer (XRD) with CuK α radiation of 0.1506 nm at a scan speed of 0.012 per min in steps of 0.01°, was used in the range between 10° and 70° for the structural analysis on the composite. The Jeol JSM-7800F Field Emission scanning electron microscope (FESEM) was used to determine of the morphological characteristics. UV–vis reflectance and absorbance data were obtained using a Lambda 950 PerkinElmer UV WinLab Spectrophotometer at wavelengths between 300 and 600 nm. A Hitachi Model F-7000 FL Spectrophotometer was used to determine the photoluminescence (PL) characteristics of the nano-powders. The Fourier transform infrared (FTIR) data was collected using a Thermo Scientific Nicolet 6700 FT-IR with NXR FT-Raman accessory system.

3 Results and discussion

The combustion rates of the reactions involving different fuels were not the same. Among the fuels used, hydrazine hydrate was most explosive with a tendency to disperse the powder through propulsion, followed closely by glycine, then citric acid, urea, and ammonium nitrate in that order.

3.1 Structural analysis on the composite from XRD

The XRD patterns obtained exhibited varying phases characterized by different intensities, full width at half maxima (FWHM) as well as shifted peak positions depending on the fuel used in the synthesis. This in turn influenced the physical, structural and optical properties of the crystallites as observed in the differences within the phase composition, crystal size, micro-strain, lattice parameters and dislocation density of the samples.

The XRD data obtained from the annealed samples was analyzed and the corresponding diffraction patterns refined by Profex, a Rietveld refinement software, then compared with the existing reference files to identify the composition of the various powders. Figure 2 shows the original and refined diffraction patterns of the samples prepared using different fuels. It was revealed that the nanocomposites consisted of zinc zirconate and zinc oxide nano-crystallites as inferred from International Centre for Diffraction Data (ICDD) reference cards 32–1482 and 75–1526, respectively. The patterns further exhibited tetragonal (t-ZrO_2) and cubic zirconia (c-ZrO_2) peaks of various intensities that corresponded to ICDD cards 80–2155 and 81–1551, respectively. The most prominent zinc oxide peaks were the (101), (100) and (110) peaks observed at 36.5°, 32.0° and 56.8°, respectively. The t-ZrO_2 (101), (112) and (211) peaks were observed at 30.4°, 50.4°, and 60.4° while the (111), (220) and (311) c-ZrO_2 peaks were detected at 30.5°, 50.7°, 60.2°, respectively. The profiles showed the best zinc zirconate ($ZnZrO_3$) peak at 27.8° in the samples prepared using hydrazine hydrate while minor peaks were seen at around 64°, 24° and 41° (ICDD 32–1482 card not indexed), making the composite of interest as a raw material in the perovskite solar cell (PSC) industry. All the major peaks in the nanocomposite XRD profile were identified.

Table 1 shows the percentage yield of each of the phases of the nanocomposites prepared using the various fuels. The percentage yield of ZnO was about 10% when citric acid, glycine and hydrazine hydrate were used as the synthesis fuels but was suppressed when either urea or its blend with ammonium nitrate was used.

Figures 2a, b show that when citric acid was used in the synthesis, the sample produced the highest yield of cubic zirconia, with the addition of ammonium nitrate to the fuel causing a slight increase in the percentage yield of t-ZrO_2 and the ZnO phases. When glycine was used as fuel, the composite produced consisted mainly of c-ZrO_2 and some t-ZrO_2 (whose yield improved when compared with the use of citric acid) while its blend with ammonium nitrate further reduced the yield of c-ZrO_2 but enhanced that of t-ZrO_2, as observed from Fig. 2c, d. Figure 2e, f show that the use of hydrazine hydrate produced still a high percentage of c-ZrO_2 as compared to the other phases and the highest yield of ZnO among the fuels used in this study. The yield of zinc zirconate was more enhanced in the blend hydrazine hydrate and ammonium nitrate. Figures 2g, h revealed that the use of urea produced only tetragonal zirconia with traces of ZnO and that the c-ZrO_2 phase was absent, while in the blend of urea with ammonium nitrate represented by 2(h), the yield of the cubic zirconia was about twice that of the tetragonal phase. The smoldering combustion involving urea as the only fuel seemed to have promoted the growth of the tetragonal phase, although the cubic phase stabilized at higher temperatures that were influenced by the presence of NH_4NO_3 [18]. The use of ammonium nitrate as the only fuel produced mostly c-ZrO_2, a little of the t-ZrO_2 phase with traces of ZnO. Further, the diminished ZnO peaks in some cases may be an indication the possibility of the formation of a ZnO-ZrO_2 solid solution [19].

For each phase, the first five major peaks were used to investigate its crystallite features. The Scherrer equation, $\beta_D = \frac{k\lambda}{D\cos\theta}$ and Bragg's equation, $n\lambda = 2d\sin\theta$ were used to determine the crystallite size, D and interplanar spacing, d, respectively. For each sample, the crystallite characteristics were calculated and tabulated in Table 2. The table further shows the dislocation density, δ, alongside the calculated and reference lattice parameters corresponding to the ICDD files

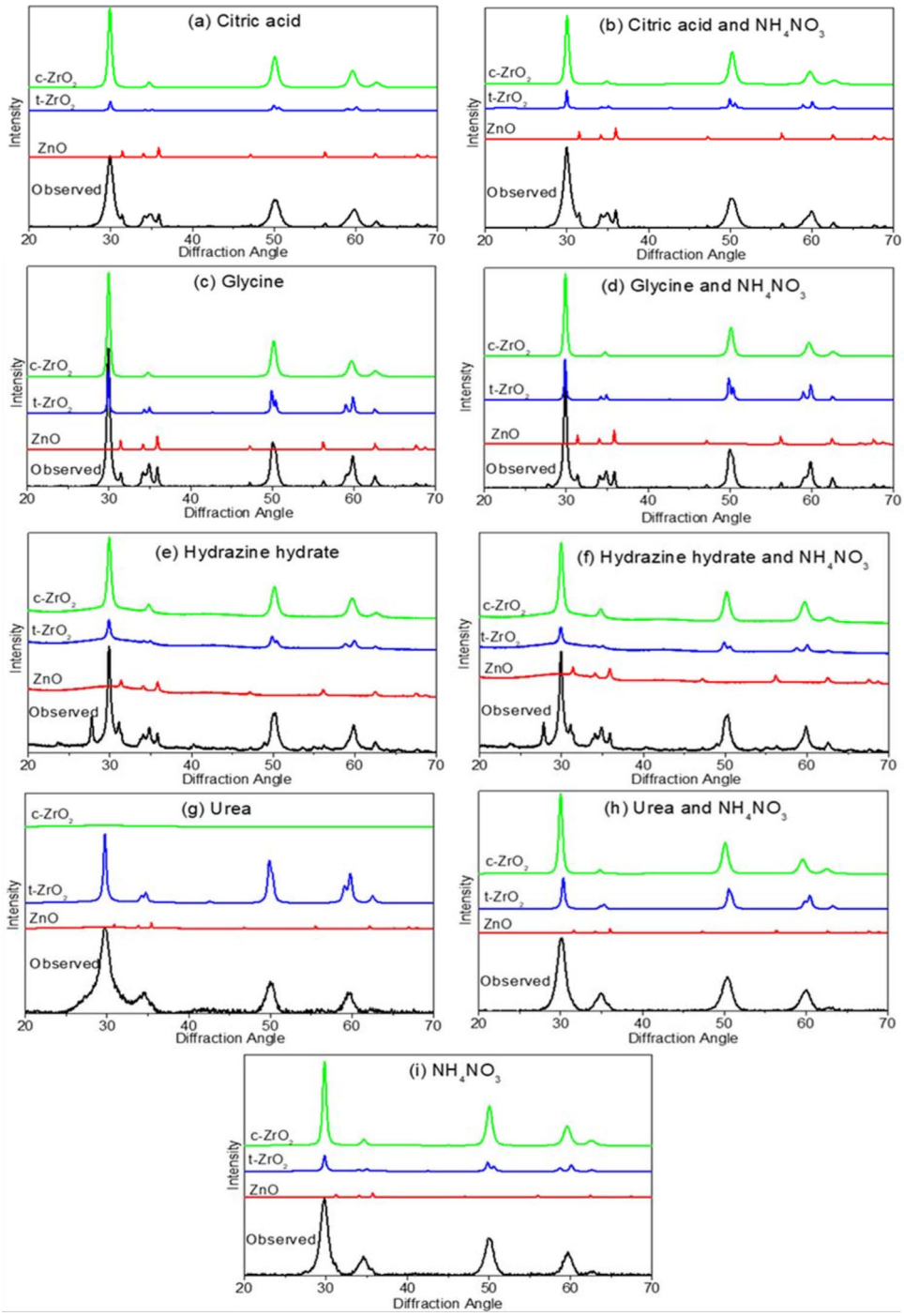

Fig. 2 The XRD patterns of the samples prepared using different fuels with the ZnO, ZrO_2 and $ZnZrO_3$ planes referenced accordingly

Table 1 Percentage yield of the composite phases synthesized using different fuels

	Citric acid	Citric + NH_4NO_3	Glycine	Glycine + NH_4NO_3	Hydrazine	Hydrazine + NH_4NO_3	Urea	Urea + NH_4NO_3	NH_4NO_3
ZnO	9.73	12.29	12.3	13.42	13.55	15.31	3.34	1.97	3.1
c-ZrO2	79	73	59.3	54.3	64.3	65.8	0	60.8	77.9
t-ZrO2	11.3	14.7	28.4	32.3	22.1	18.9	96.66	37.2	19

Table 2 The average values of the crystallite size D, the lattice parameters and the dislocation density, δ (in 10^{-4} nm^{-2}) of the composite phases prepared using different fuels

	ZnO				c-ZrO_2			t-ZrO_2			
Lattice parameters	a (10^{-1} nm)	c (10^{-1} nm)	D (nm)	δ	a (10^{-1} nm)	D (nm)	δ	a (10^{-1} nm)	c (10^{-1} nm)	D (nm)	δ
Reference files	3.243	5.195	–		5.159	–		3.607	5.129	–	
Citric acid	3.253	5.223	80.05	1.56	5.120	22.85	19.1	3.586	5.190	41.28	5.87
Citric + NH_4NO_3	3.254	5.215	78.58	1.62	5.115	22.82	19.2	3.593	5.203	59.03	2.87
Glycine	3.256	5.204	80.08	1.56	5.115	27.50	13.2	3.600	5.185	58.19	2.95
Glycine + NH_4NO_3	3.254	5.213	80.06	1.56	5.115	29.05	11.8	3.598	5.187	56.90	3.09
Hydrazine	3.260	5.212	42.61	5.51	5.115	20.55	23.7	3.595	5.202	32.65	9.38
Hydrazine + NH_4NO_3	3.259	5.210	41.11	5.92	5.115	21.82	21.0	3.591	5.216	29.98	11.1
Urea	3.282	5.212	178.8	0.31	–	–	–	3.594	5.161	27.29	13.4
Urea + NH_4NO_3	3.257	5.221	124.5	0.65	5.138	22.85	19.1	3.580	5.132	29.45	11.5
NH_4NO_3	3.263	5.205	74.88	1.78	5.115	22.34	20.0	3.581	5.211	34.85	8.24

The gaps in the entries are for the phases that were not detectable or missing altogether

for the hexagonal ZnO and the ZrO_2 phases. From the table, it was observed that the lattice parameters of each sample were slightly larger than those in the reference cards, probably because of the peak shifts arising from the presence of the other phases in the composite.

Studies on the stoichiometric use of urea have shown that synthesized particles are characterized by poor crystallinity and low purity [20]. From Table 2, it is observed that the use of urea as the only fuel produced the smallest crystallites of the t-ZrO_2 phase. The high abundance of the tetragonal phase (97%) in the composite (Table1), may explain the XRD peak broadening that was observed in the profile presented in Fig. 2h compared with the rest of the samples. On the contrary, some other studies have shown that urea tends to promote the precipitation of metal cations inside the gel, leading to the nucleation of the particles as well as extended agglomeration after combustion which may explain the large ZnO crystallites. Compared to the other fuels used in the synthesis, the explosive combustion involving hydrazine hydrate produced smaller particles than the rest probably because of the dispersion produced by the generated gases [14].

The properties of a material can be greatly influenced by the presence of dislocations in its structure. A dislocation arises from irregularities within the crystal structure that are formed through inhomogeneous nucleation, grain boundary initiation or lattice interface with other defects including dispersed phases. The dislocation density, δ of a crystal is expressed as $\delta = \frac{1}{D^2}$, hence materials with smaller crystallites are characterized by a larger dislocation density [21, 22]. Studies have shown that the higher the dislocation density, the harder the material and the lower the strain in the material [22]. Such substances are further characterised by high specific surface area and are likely to have better adsorption properties. These dislocations constitute of electron traps that may affect both thermal and electrical properties like conductivity, energy band gap as well as the photoactivity of the material [23]. It was observed that the samples prepared using hydrazine hydrate had the highest dislocation density probably due to the explosive nature of the combustion reaction involved.

3.2 Morphology studies

Figure 3 shows selected SEM images of the synthesized nanocomposites. In Fig. 3a, the composite material that was synthesized using citric acid seemed to crack exposing regular polygonal aggregates as well as some highly agglomerated regions. Figure 3b shows the formation of closely packed large aggregates of various shapes that were produced when urea was used as fuel. In the synthesis involving hydrazine hydrate fuel, a high density of standing nanorods was observed in Fig. 3c. Figure 3d shows a highly porous material exhibiting a spongy agglomerated mesh of underlying crystals that was formed when glycine was used in the synthesis as a fuel. Figure 3e shows that the use of a blend of glycine and ammonium nitrate produced small polygonal particles that seemed to have been dispersed from cracks within an underlying encapsulating spongy sheet below the particles. The formation of the aggregates concurs with reports that there is less agglomeration of particles when ammonium nitrate is blended with any of the fuels [6]. The micrographs show a greater dispersion and increased surface area of the particles when glycine and hydrazine are involved due to the enhanced gas

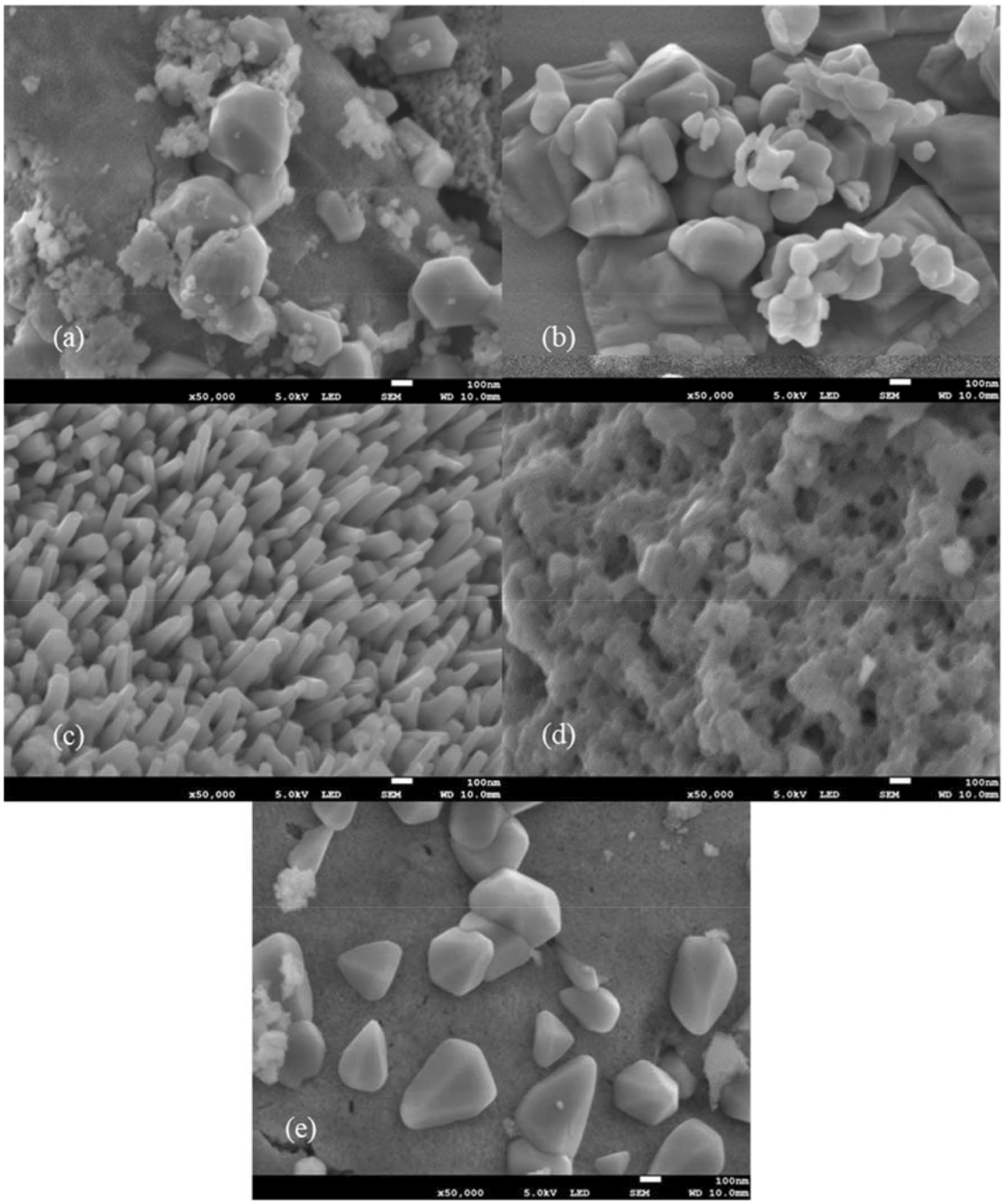

Fig. 3 SEM morphology images of samples synthesized using **a** citric acid **b** urea **c** hydrazine hydrate **d** glycine **e** blend of glycine and ammonium nitrate fuels

evolution during their synthesis and, therefore, confirm the influence of the type of fuel on the morphology of the particles formed. These highly porous nanocomposites may be applied in photocatalysis and water treatment industry because of their large surface area-volume ratio.

3.3 FTIR spectroscopy

The Fourier Transform Infrared (FTIR) spectroscopy test was done to establish whether any undesired precursor, remnant fuels or other compounds that arose from sample preparation were still present in the material necessitating any further heat treatment. Several studies have indicated

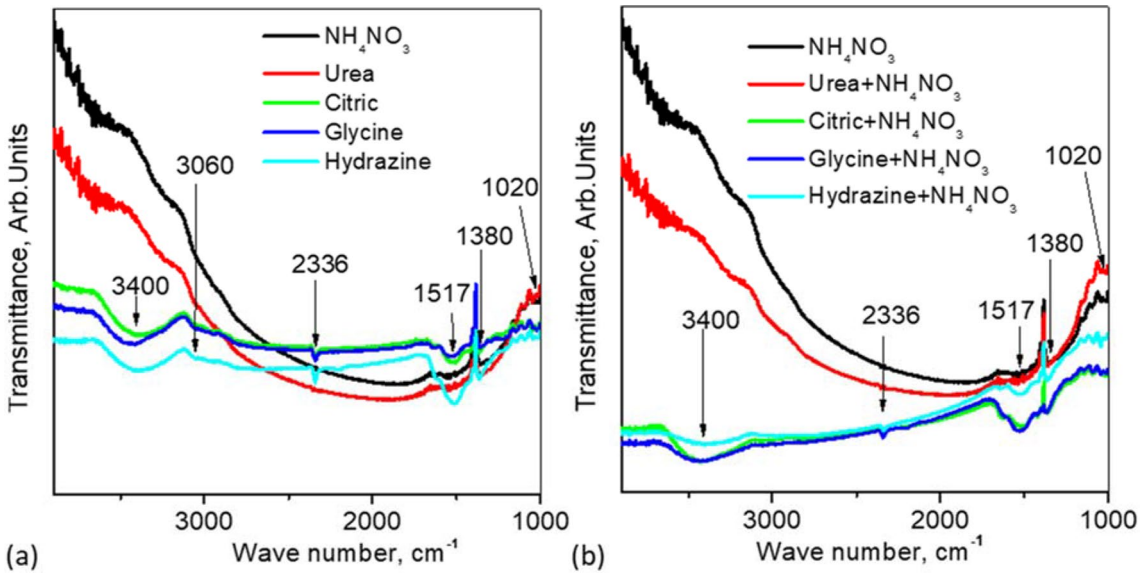

Fig. 4 The FTIR spectrum showing absorption peaks of the functional groups present in the samples prepared using **a** single fuels **b** ammonium nitrate in addition to the fuel

that the IR spectrum range between 1300 and 4000 cm^{-1} is the most useful region for the identification of any functional group of compounds within a given material [24, 25].

Based on ammonium nitrate as the reference, Fig. 4a shows the FTIR spectra of the nanocomposites synthesized by the various single fuels while Fig. 4b shows the spectra when the fuels were blended with NH_4NO_3. From the spectra, no major identifiable absorption peaks were observed when the synthesis involved urea, ammonium nitrate or their blend probably because of their low reducing valences and the lack of any carbonaceous residue within the synthesized materials [15].

The broad shallow IR absorption peaks seen around 3400 and 1517 cm^{-1} were associated with the stretching and bending vibrations due to hydroxyl bonds connected to the Zr^{4+} ions [19, 26–28]. There is a possibility, however, that the ethanol used in sample preparation during the analysis or absorbed moisture contributed to this peak. A narrow band was observed at 2336 cm^{-1} suggesting the presence of carboxylic stretching frequencies while the band seen at 1380 cm^{-1} was attributed to N–O bonds within the material [20]. The absorbance at 3060 cm^{-1} further confirms the presence of the OH^- bonds while the band at 1020 cm^{-1} may be due to the Zr-O stretching bond frequencies [26, 29]. The peaks observed in these FTIR spectra were minor, indicating that there were no major residues present in the samples and hence no further heat treatment was deemed necessary [15]. In Fig. 4b, the use of NH_4NO_3 was observed to produce a decrease in the intensity of the transmittance from the nanocomposites. This was attributed to the coarse nature of the powders as well as the larger crystallite sizes of the most abundant c-ZrO_2 phase that caused less diffuse reflectance from the crystals as compared to the other samples [30].

3.4 UV–vis spectroscopy

Figure 5 shows the UV–vis reflectance spectra based on ammonium nitrate as a reference for the samples synthesized using different fuels. The UV–vis reflectance curves show variations in both the shape and position of the absorption edges obtained from the samples combusted with different fuels. At longer wavelengths, the samples synthesized using citric acid and those involving glycine had a greater reflectance while those based on urea had the least. When the fuels were blended with ammonia nitrate, it was observed in Fig. 5b that there was reduced reflectance compared with the non-blended fuels in 5a.

According to Zhu et al. [31], major absorption edges can be found by extrapolating the sharply dropping sections of the absorption spectra to the *x*-axis. For these nanocomposites, the edges spread between 396 and 440 nm depending on the type of fuel used [26, 31]. There were minor absorption peaks in some of the powders around 455 and 496 nm that correlated to the peaks observed in PL spectroscopy.

Figure 6 shows graphs of the Kubelka–Munk function, $F(R)$, on which $[F(R)hv]^2$ was plotted against the photon energy, hv. By the use of ammonium nitrate as a reference, Fig. 6a shows the spectra from the samples prepared from the single fuels while Fig. 6b represents those in which the fuels were blended with ammonium nitrate. By extrapolating the linear sections to the *x*-axis, the figures were used to determine the energy bandgap of the samples.

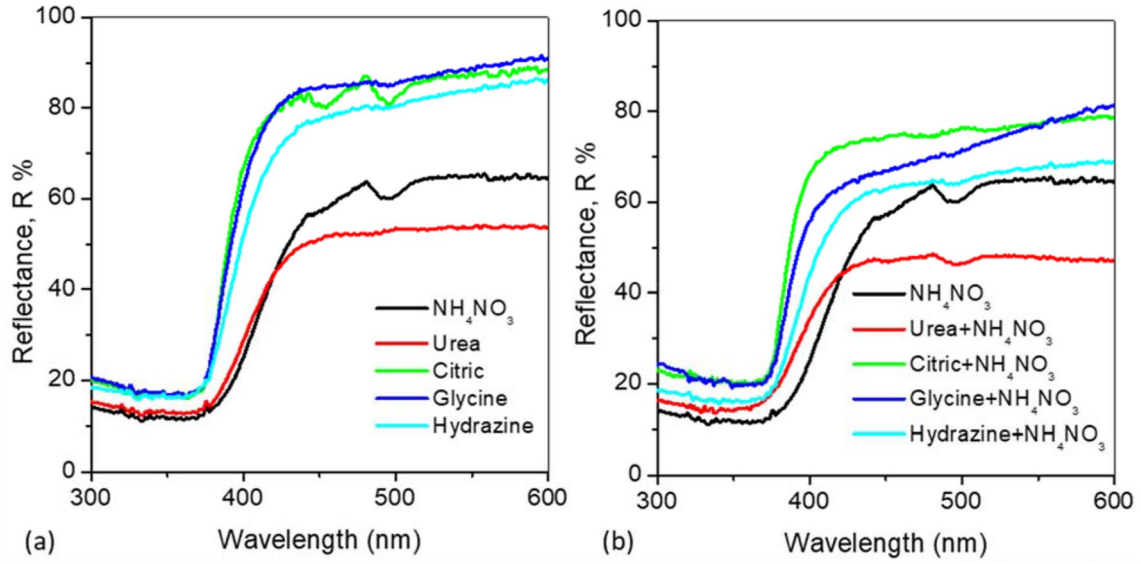

Fig. 5 UV–vis reflectance spectra of the samples prepared using different fuels

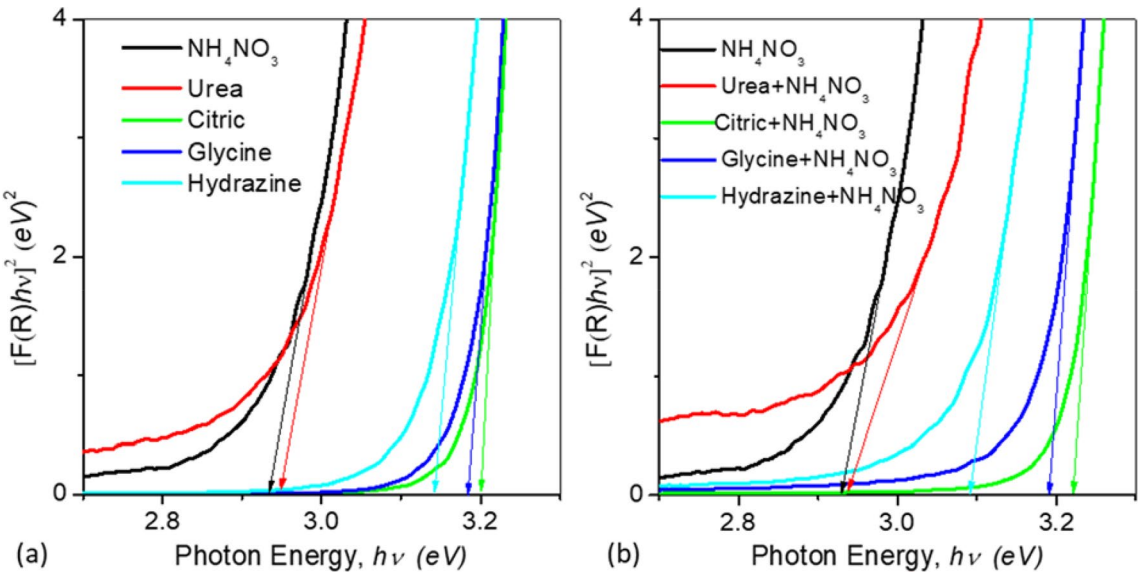

Fig. 6 Plots of the Kubelka–Munk function that were used to obtain the energy bandgap of the samples for **a** single fuels **b** blended fuels

Table 3 Values of the energy bandgaps (*eV*) for the nanocomposites synthesized using various fuels

Type of fuel	NH_4NO_3	Urea	Citric	Glycine	Hydrazine
Without NH_4NO_3	–	2.95	3.20	3.18	3.14
With NH_4NO_3	2.93	2.94	3.22	3.19	3.09

Table 3 shows that the calculated energy band gaps of the samples were between 2.93 and 3.22 eV. These results show that the bandgap is dependent on the type of fuel used in the synthesis of that material. It was noticed the energy band gap of the samples synthesized using urea and/or ammonium nitrate were considerably lower than those of the rest of the fuels.

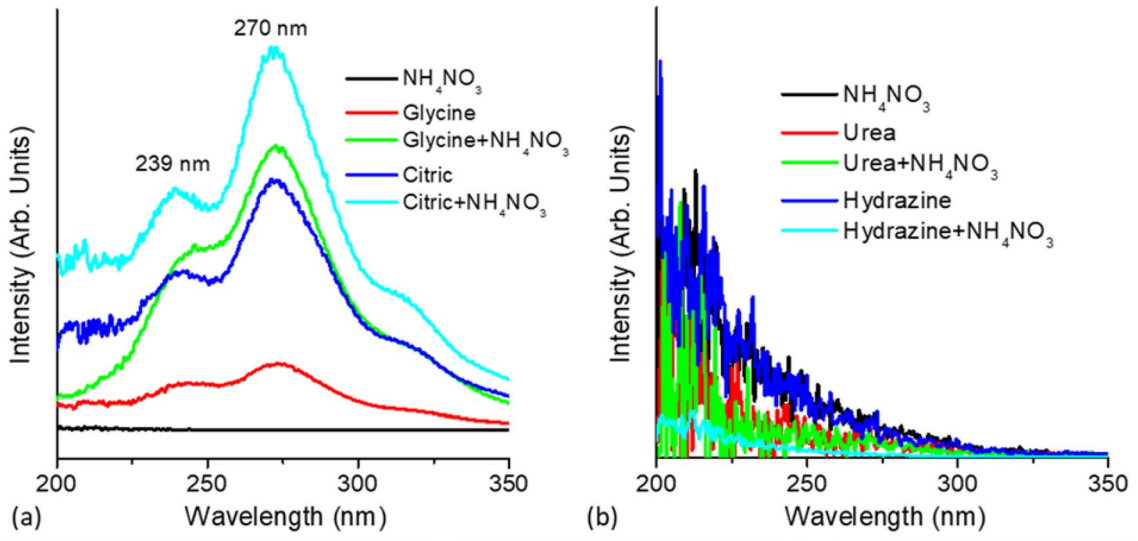

Fig. 7 **a** Excitation photoluminescence spectra of the samples synthesized using citric acid and glycine **b** negligible excitation spectra from urea and hydrazine-based samples

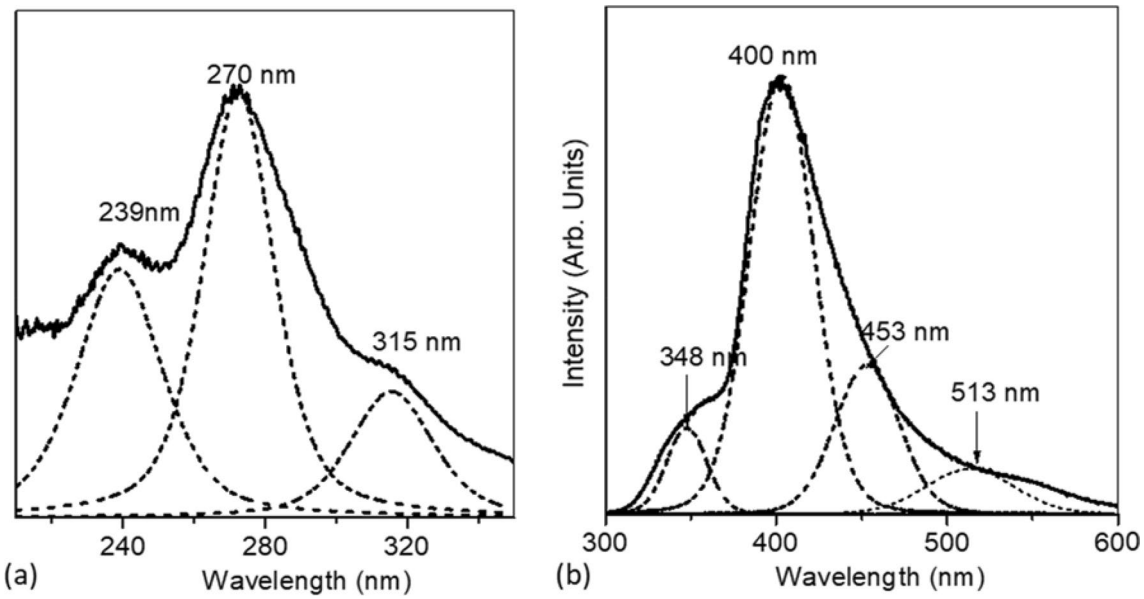

Fig. 8 Deconvolution of the most intense **a** excitation **b** emission peaks involving citric acid blended with ammonium nitrate

3.5 Photoluminescence analysis

Figure 7 shows the excitation spectrum of the samples prepared using different fuels when probed at 400 nm. In Fig. 7a, the spectra from the samples that were synthesized using either citric acid or glycine produced peaks of the same form but different intensities, while those from urea and hydrazine showed insignificant peaks (Fig. 7b). The highest photoluminescent intensity was observed in the sample prepared using a blend of citric acid and ammonium nitrate followed by that which used glycine and ammonium nitrate. These diverse intensities were attributed to the differences in crystal sizes as well as the variations in the morphology of the samples. Figure 8 shows the deconvolution of the broad excitation and emission peaks. In Fig. 8a, deconvoluted excitation peaks were observed at about 239 nm and the most dominant one at around 270 nm with a minor one seen at 315 nm. These emissions were attributed to the band to band transitions, defects

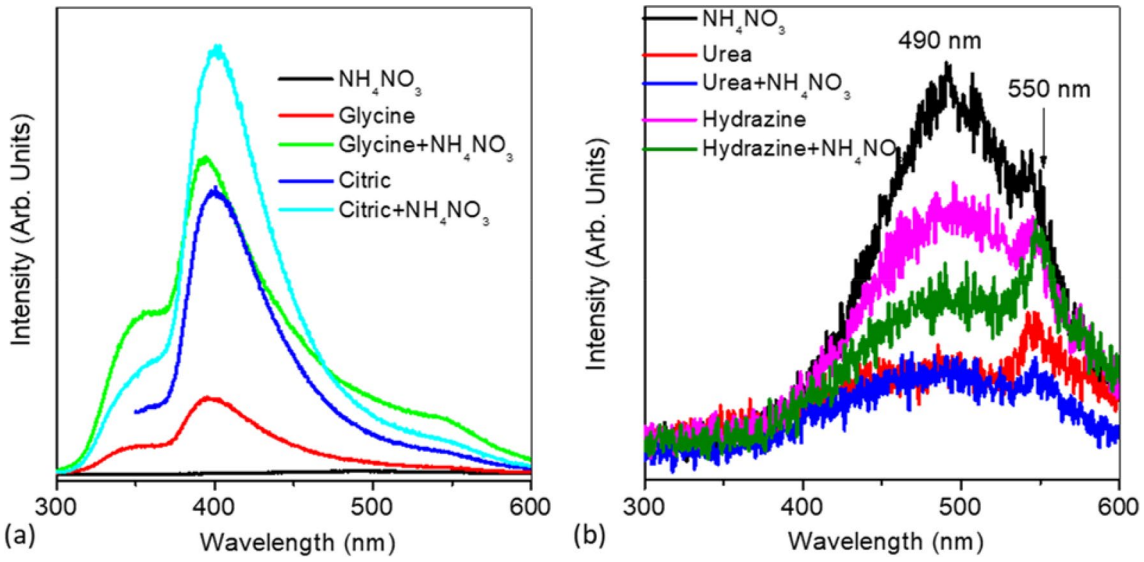

Fig. 9 **a** Emission photoluminescence spectra of the samples synthesized using citric acid and glycine **b** low emission spectra from urea and hydrazine—based samples

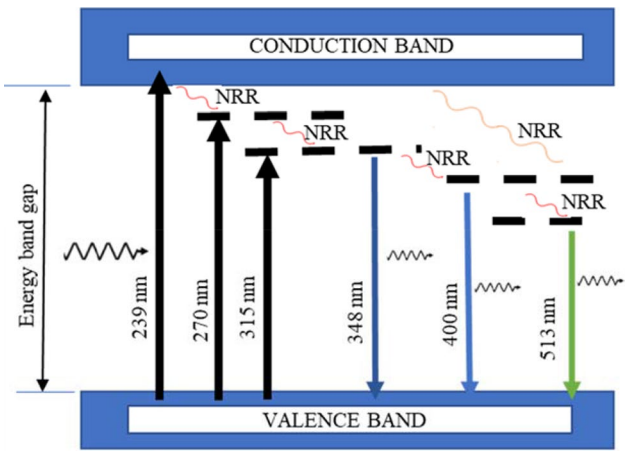

Fig. 10 The energy transitions taking place within the nanocomposite material

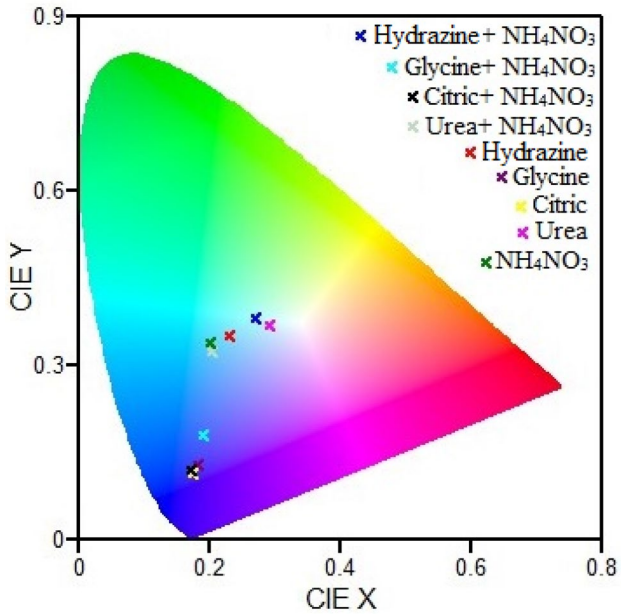

Fig. 11 CIE diagram showing the colors emitted by the composites prepared using different fuels

within ZrO_2 and ZnO lattices within the composite material, respectively [17, 19].

Figure 9a shows the emission spectra of the samples synthesized using citric acid and glycine. On deconvolution of the spectra, the most intense peak at 400 nm in Fig. 8b was attributed to transitions in the zinc oxide phase. The other peaks observed at 348, 453 and 513 nm were associated with emissions from the zinc zirconate phase [32], the ionized zinc vacancies [33] and the defect levels within the ZnO valence band [34], respectively. For the samples synthesized using either urea or hydrazine hydrate (Fig. 9b) the peaks were broader and of relatively lower intensity compared to those prepared with other fuels. In these samples, the peaks observed at 490 and 550 nm were attributed to the zirconia and zinc zirconate phases, respectively. These latter peaks confirm the absence or negligible presence of the zinc oxide phase in the samples as observed in Fig. 2 and Table 1; further collaborating the varied band gap seen in Fig. 6. When the PL spectroscopy is used to calculate the band gap, a value of 3.1 eV is obtained, which agrees quite well with the UV spectroscopy.

It was observed from the spectroscopy graphs that the synthesis involving NH_4NO_3 produced lower intensities

as compared to the rest. This was attributed to the reduced agglomeration and hence more defined grain boundary defects that act as traps within the structure, compounded by the general increase in the crystal size of the more abundant cubic zirconia. The energy diagram in Fig. 10 illustrates the excitonic band–band and near band photoluminescent emissions taking place within the composite material.

Figure 11 shows the CIE coordinate diagram of the composite. The diagram represents the chromaticity coordinates determined for the composite samples obtained using the Commission International de I'Eclairage (CIE) Coordinate Calculator software [35]. The coordinates of the samples traverse the violet-blue color into the yellow-white region. The spread of the emissions on the diverse colors was an indication of the influence of the fuels on the luminescence properties of the phosphor nanocomposites. As such the phosphors can be used in light emitting diodes (LEDs), varied color sensors and in efficient white-light applications.

4 Conclusion

Zinc zirconate nanocomposites were synthesized successfully using different fuels through the solution combustion route. Depending on the fuel used in the synthesis, the nanocomposites consisted of mixed phases of zinc zirconate, zinc oxide, cubic and tetragonal zirconia. The zinc zirconate peaks were better formed when hydrazine hydrate and glycine were used as the synthesis fuels. The synthesis involving urea or ammonium nitrate mainly produced the tetragonal zirconia and a little zinc oxide. For the samples synthesized with citric acid and glycine, the most prominent emission peak was observed at 400 nm while for hydrazine hydrate and urea it was at 490 nm. This investigation has therefore shown that the structural and optical characteristics of the synthesized zinc zirconate nanocomposites depend on the type of fuel used. The nanocomposites may be applied in many sectors such as water treatment, PSC industry, sensors and LEDs.

Acknowledgements We are grateful to the University of the Free State and the National Research Fund, NRF South Africa for facilitating the study.

References

1. A. Pivkina, P. Ulyanova, Y. Frolov, S. Zavyalov, J. Schoonman, Nanomaterials for heterogeneous combustion. Propellants Explos. Pyrotech. **29**, 39–48 (2004)
2. N. Assi, A.A.M. Sharif, Q.S.M. Naeini, Synthesis, characterization and investigation photocatalytic degradation of Nitro Phenol with nano ZnO and ZrO_2. Int. J. Nano Dimens. **52014**, 387–391 (2014)
3. P. Palmero, Structural ceramic nanocomposites: a review of properties and powders' synthesis methods. Nanomaterials **5**, 656–696 (2015)
4. E.T. Thostenson, C. Li, T.-W. Chou, Nanocomposites in context. Compos. Sci. Technol. **65**, 491–516 (2005)
5. L.L. Beecroft, C.K. Ober, Nanocomposite materials for optical applications. Chem. Mater. **9**, 1302–1317 (1997)
6. A.K. Alves, C.P. Bergmann, F.A. Berutti, Combustion synthesis, *Novel Synthesis and Characterization of Nanostructured Materials* (Springer, Berlin, 2013), pp. 11–22
7. A.R. West, *Solid State Chemistry and its Applications*, 2nd edn. (Department of Materials Science and Engineering, University of Sheffield, John Wiley & Sons Ltd, UK, 2005)
8. T. Mimani, K.C. Patil, Solution combustion synthesis of nanoscale oxides and their composites. Mater. Phys. Mech. **4**, 134–137 (2001)
9. A. Varma, A.S. Mukasyan, A.S. Rogachev, K.V. Manukyan, Solution combustion synthesis of nanoscale materials. Chem. Rev. **116**, 14493–14586 (2016)
10. A.S. Mukasyan, P. Epstein, P. Dinka, Solution combustion synthesis of nanomaterials. Proc. Combust. Inst. **31**, 1789–1795 (2007)
11. K.C. Patil, M.S. Hegde, T. Rattan, S.T. Aruna, Chemistry of nanocrystalline oxide materials world, *Solution Combustion Synthesis of Oxide Materials* (Scientific Publishing Co. Pte. Ltd., Singapore, 2008), pp. 42–60
12. S. Challagulla, S. Roya, The role of fuel to oxidizer ratio in solution combustion synthesis of TiO_2 and its influence on photocatalysis. J. Mater. Res. **32**, 2764–2772 (2017)
13. F. Deganello, G. Marcìb, G. Deganello, Citrate–nitrate auto-combustion synthesis of perovskite-type nanopowders: a systematic approach. J. Eur. Ceram. Soc. **29**, 439–450 (2009)
14. F. Deganello, A.K. Tyagi, Solution combustion synthesis, energy and environment: best parameters for better materials. Prog. Cryst. Growth Charact. Mater. **64**, 23–61 (2018)
15. S.L. González-Cortés, F.E. Imbert, Fundamentals, properties and applications of solid catalysts prepared by solution combustion synthesis (SCS). Appl. Catal. A **452**, 117–131 (2013)
16. F.-T. Li, J. Ran, M. Jaroniec, S.Z. Qiao, Solution combustion synthesis of metal oxide nanomaterials for energy storage and conversion. Nanoscale **7**, 17590–17610 (2015)
17. M.K. Musembi, F.B. Dejene, Investigation of the effect of precursor ratios on the solution combustion synthesis of zinc zirconate nanocomposite. Heliyon **5**, e03028 (2019)
18. I. Ahemen, F. Dejene, Photophysical and energy transfer processes in Ce^{3+} co-doped ZrO_2: Eu^{3+} nanorods. Appl. Phys. A **123**, 140–147 (2017)
19. T. Ivanova, A. Harizanova, T. Koutzarova, B. Vertruyen, Effect of annealing temperatures on properties of sol-gel grown ZnO-ZrO_2 films. Cryst. Res. Technol. **45**, 1154–1160 (2010)
20. L.S. Carvalho, VRdMe Melo, DMdA Melo, E.V. Sobrinho, D. Ruiz, Effect of urea excess on the properties of the $MgAl_2O_4$ obtained by microwave-assisted combustion. Mater. Res. **21**, 11 (2018)
21. K.A. Aly, N.M. Khalil, Y. Algamal, Q.M.A. Saleem, Estimation of lattice strain for zirconia nano-particles based on Williamson-Hall analysis. Mater. Chem. Phys. **193**, 182–188 (2017)
22. T. Theivasanthi, M. Alagar, Titanium dioxide (TiO_2) nanoparticles XRD analyses: an insight. Mater. Sci. **1**, 1–10 (2013)
23. D.B. Sirdeshmukh, L. Sirdeshmukh, K.G. Subhadra, The physics of mixed crystals, *Micro- and Macro-Properties of solids: Thermal, Mechanical and Dielectric properties* (Springer, Berlin, 2006), pp. 285–327
24. B. Schrader, General survey of vibrational spectroscopy, in *Infrared and Rarnan Spectroscopy Methods and Applications, B*, ed. by Ed Schrader (VCH Verlagsgesellschaft mbH, VCH Publishers, Weinheini, 1995), pp. 7–61

25. H. Mark, Fundamentals of NIR spectroscopy, in *Near-Infrared Applications in Biotechnology, R*, ed. by Ed Raghavachari (CMarcel Dekker Inc, New York, 2001), pp. 293–321
26. M.H. Habibi, E. Askari, Thermal and structural studies of zinc zirconate nanoscale composite derived from sol–gel process. The effects of heat-treatment on properties. J. Therm. Anal. Calorim. **111**, 227–233 (2013)
27. M.H. Habibi, E. Askari, Fabrication and spectral properties of zinc zirconate nanorod composites by sol-gel method for optical applications: effect of chloride and oxychloride precursors and sintering temperature on band gap. Synth. React. Inorg. Met. Org. Nano-Met. Chem. **45**, 281–285 (2015)
28. M.C.U. López, M.A.A. Lemus, M.C. Hidalgo, R.L. González, P.Q. Owen, S. Oros-Ruiz et al., Synthesis and characterization of ZnO-ZrO_2 nanocomposites for photocatalytic degradation and mineralization of phenol. J. Nanomater. **12**, 1 (2019)
29. I. Ahemen, F.B. Dejene, R. Botha, Strong green-light emitting Tb^{3+} doped tetragonal ZrO_2 nanophosphors stabilized by Ba^{2+} ions. J. Lumin. **201**, 303–313 (2018)
30. E.A.C. Miranda, J.F.M. Carvajal, O.J.R. Baena, Effect of the fuels glycine, urea and citric acid on synthesis of the ceramic pigment $ZnCr_2O_4$ by solution combustion. Mater. Res. **18**, 1038–1043 (2015)
31. X. Zhu, J. Zhou, J. Zhu, Z. Liu, Y. Li, T. Al-Kassab, Structural characterization and optical properties of perovskite $ZnZrO_3$ nanoparticles. J. Am. Ceram. Soc. **97**, 1987–1992 (2014)
32. M.H. Habibi, E. Askari, M. Habibi, M. Zendehdel, Novel nanostructure zinc zirconate, zinc oxide or zirconium oxide pastes coated on fluorine doped tin oxide thin film as photoelectrochemical working electrodes for dye-sensitized solar cell. Spectrochim. Acta Part A Mol. Biomol. Spectrosc. **104**, 197–202 (2013)
33. R.K. Biroju, P.K. Giri, Strong visible and near infrared photoluminescence from ZnO nanorods/nanowires grown on single layer graphene studied using sub-band gap excitation. J. Appl. Phys. **122**, 11 (2017)
34. O. Yayapao, T. Thongtemb, A. Phuruangrat, S. Thongtem, Sonochemical synthesis of Dy-doped ZnO nanostructures and their photocatalytic properties. J. Alloy. Compd. **576**, 72–79 (2013)
35. P. Patil. (2010) CIE coordinate calculator. Available: https://www.mathworks.com/matlabcentral/fileexchange/29620-cie-coordinate-calculator. Accessed 15 Mar 2020